Effects of Alloyed and Oxide Phases on Methanol Oxidation of Pt–Ru/C Nanocatalysts of the Same Particle Size

ARTICLE *in* THE JOURNAL OF PHYSICAL CHEMISTRY C · MAY 2009

Impact Factor: 4.77 · DOI: 10.1021/jp8108804

3 AUTHORS:

Denis Martins de Godoi
São Paulo State University
15 PUBLICATIONS **157** CITATIONS
SEE PROFILE

Joelma Perez
University of São Paulo
43 PUBLICATIONS **997** CITATIONS
SEE PROFILE

Hebe de las Mercedes Villullas
São Paulo State University
44 PUBLICATIONS **709** CITATIONS
SEE PROFILE

Effects of Alloyed and Oxide Phases on Methanol Oxidation of Pt−Ru/C Nanocatalysts of the Same Particle Size

Denis R. M. Godoi, Joelma Perez, and H. Mercedes Villullas*

Departamento de Físico-Química, Instituto de Química, Universidade Estadual Paulista (UNESP), 14801-970 CP 355, Araraquara, Brazil

Received: December 10, 2008; Revised Manuscript Received: March 30, 2009

In this work, methanol oxidation was studied on carbon-supported Pt−Ru nanocatalysts, where the amounts of alloyed and oxide phases were modified by heat treatments in different atmospheres. Because particle growth was avoided using mild temperature conditions, the study reported here was conducted in the absence of particle size effects. All samples were characterized by X-ray diffraction and transmission electron microscopy. The general electrochemical behavior of the nanocatalysts was evaluated by cyclic voltammetry, and the electrocatalytic activity for the oxidation of methanol was studied in 0.5 mol L^{-1} methanol acid solutions by linear potential sweeps and chronoamperometry. The results obtained clearly evidence that the presence of oxide species is necessary to enhance the electrocatalytic activity for methanol oxidation. Oxidation of adsorbed CO was also measured. Both reactions, methanol and adsorbed CO oxidation, were found to be very sensitive to the surface changes produced by the heat treatments. Interestingly, the best catalyst for methanol oxidation was not found to be the most efficient for the oxidation of adsorbed CO. Electrocatalytic activities correlate well with oxidation states and electronic properties analyzed by X-ray photoelectron spectroscopy and in situ dispersive X-ray absorption spectroscopy.

Introduction

The use of fuel cells for the production of electric power in a clean, silent, and efficient way comes as an excellent alternative for supplying part of the current needs of energy production.[1,2] Proton exchange membrane fuel cells (PEMFC) are among the most promising of those devices, and the most efficient ones generate electric power from the oxidation of hydrogen in the anode and reduction of oxygen in the cathode.

While direct methanol fuel cells (DMFC) are alternative systems for replacing hydrogen by a liquid fuel because they minimize storage and transport problems and eliminate the need of a reformer, several problems remain to be solved to make DMFC performance sufficient for many practical applications. Among them, the performance of the catalysts still needs to be improved. Even though Pt is the most active metal for the electrochemical oxidation of methanol,[3] the slow kinetics of the reaction and the formation of strongly adsorbed intermediates such as carbon monoxide produce substantial losses in operation potentials. The most common approach to this problem has been the development of Pt-based catalysts such as Pt−Ru, Pt−Mo, Pt−Ni, etc.[3−15] The enhanced activity of these materials is generally interpreted in terms of the ability of the second metal to supply, in lower potentials, the oxygenated species necessary for the complete oxidation of the alcohol and for the removal of the poisoning species adsorbed onto the catalyst surface.[16] Additionally, electronic effects have also been attributed to the second metal, which would result in weakening the bond between the poisoning species and catalyst surface.[17]

Published results show that methanol oxidation on Pt−Ru is greatly influenced by a number of physical properties such as composition, structure, morphology, particle size, and degree of alloying. It was also shown that those properties depend on synthesis conditions, and therefore, it is not surprising to find that the electrocatalytic activity is also strongly dependent on the preparation methodology adopted.[18] In a recent work by our group,[19] properties such as the degree of alloying and amount of oxides were determined for Pt−Ru/C nanocatalysts, which were synthesized in water/*n*-heptane/AOT microemulsions with their average particle size carefully controlled, were found to be size-dependent. Thus, a better understanding of the effects of structural and chemical properties seems essential to improve the electrocatalysis of methanol oxidation and as a basis for developing new and more efficient materials.

In this work, methanol oxidation was studied on Pt−Ru/C catalysts heat treated in mild temperature conditions, which did not cause any significant particle growth, and under different atmospheres that promoted changes in the amount of oxides and degree of alloying. Considerable differences in electrocatalytic activities toward methanol and adsorbed CO oxidation were observed on these Pt−Ru/C catalysts of the same particle size; they are discussed here in terms of surface composition (oxide and alloy).

Experimental Section

Electrocatalysts Preparation. Pt−Ru nanoparticles were first obtained in water/*n*-heptane/AOT microemulsions as described elsewhere.[19] Briefly, an aqueous solution of H_2PtCl_6 and $RuCl_3$ (0.5 wt % metal, Pt:Ru atomic ratio 1:1) was added to a mixture of *n*-heptane and AOT (15 wt %) under constant stirring to form a microemulsion with a water to surfactant molar ratio (*w*) equal to 8. Reduction of metallic precursors was done by adding $NaBH_4$ as a solid in a molar ratio of 10:1 to metals. The mixture was kept under constant stirring for 2 h, and then an appropriate amount of high surface area carbon (Vulcan XC-72, Cabot) was added to obtain the supported catalysts with a metal load (Pt + Ru) of 20 wt %. The suspension obtained was stirred overnight.

* To whom correspondence should be addressed. E-mail: mercedes@iq.unesp.br. Fax: +55 16 3301 6692.

10.1021/jp8108804 CCC: $40.75
Published on Web 04/15/2009

TABLE 1: Heat Treatment Conditions for Pt−Ru/C Catalysts

sample	T (°C)	time (h)	atmosphere
A1[a]	80	1	air
A2	80	24	air
A3	150	1	air
B	150	1	N_2
C	150	1	H_2

[a] The as-prepared sample.

The carbon-supported catalysts were filtered, washed copiously with ethanol, acetone, and ultrapure water, and dried in air at 80 °C for 1 h (sample A1, as prepared). All reagents were purchased from Aldrich and used without further purification.

Thermal Treatments. For Pt−Ru/C catalysts prepared in microemulsions, we have recently found that differential scanning calorimetry (DSC) data taken in N_2 showed an initial endothermic loss between ambient temperature and approximately 100 °C, followed by an exothermic sharp peak, involving two partially overlapped processes, which are completed at ≈150 °C.[19,20] On the basis of the DSC results previously reported for $RuO_2 \cdot nH_2O$,[20] the endothermic loss was interpreted as the removal of physically adsorbed water, and the first component of the exothermic peak was interpreted as the accommodation of the hydrous oxide structure to the loss of water. The second process of the exothermic event, also observed for Pt/C samples,[19,20] is likely due to a crystalline transition of Pt.[21] Therefore, the as-prepared sample A1 was divided into five parts to be heat treated. Temperatures were chosen on the basis of the occurrence of the processes of loss of adsorbed water (80 °C) and structural transitions (150 °C).[19,20] Temperature and time of treatment were varied for samples treated in air, while three different atmospheres (air, nitrogen, and hydrogen) were used for treatment at 150 °C. Conditions for heat treatment of the different Pt−Ru/C catalysts are summarized in Table 1.

Electrocatalysts Characterization. A Philips CM200 instrument, operating at 200 kV, and equipped with energy dispersive spectroscopy (EDS) for energy dispersive X-ray analysis was used for the transmission electron microscopy (TEM) study and EDX analysis. X-ray diffraction (XRD) analysis was performed using a Rigaku, model D Max 2500 PC diffractometer. X-ray diffractograms with a scan rate of 1° min^{-1} and an incident wavelength of 0.15406 nm (Cu Kα) were recorded for 2θ values between 20° and 100°. In order to improve the fitting of the (220) peak, recordings for 2θ values from 60° to 80° were done at 0.02° min^{-1}.

X-ray photoelectron spectroscopy (XPS) analysis was carried out using a commercial spectrometer (UNI-SPECS UHV). The Mg Kα line was used ($h\nu = 1253.6$ eV), and the analyzer pass energy was set to 10 eV. The inelastic background of the O 1s, Pt 4f, and Ru 3p electron core level spectra was subtracted using Shirley's method. The composition of the surface layer was determined from the ratio of the relative peak areas corrected by sensitivity factors of the corresponding elements. The spectra were fitted without placing constraints using multiple Voigt profiles. The full width at half-maximum (fwhm) varied between 1.6 and 2.0 eV, and the accuracy of the peak positions was ±0.1 eV.

In situ dispersive X-ray absorption spectroscopy (DXAS) experiments were performed for some samples at the DXAS beamline of the Brazilian Synchrotron Light Laboratory (LNLS), Brazil.[22] The storage ring was operated at an energy of 1.37 GeV and an initial beam current of 240 mA. An X-ray beam with a bandwidth of a few hundred electron volts around the Pt L_3 edge (11564.25 eV) was selected using a curved Si(111) crystal monochromator. Its bending mechanism focused the beam at the sample position, and the transmitted beam was collected by using a CCD camera. The exposure time was set for 150 ms for each measured spectrum. In order to improve the signal-to-noise ratio, 100 accumulations (frames) composed a full spectrum with 1.5 s of total acquisition time. Conversion of data, pixel to energy, was performed by comparing measurements in conventional mode with those in dispersive mode from standard foils (Pt metal). The measurements were carried out in a spectroelectrochemical cell,[23] using the catalysts in the form of pellets that were prepared by pressing a mixture of Nafion solution and catalyst powder (Pt load was 6 mg cm^{-2}). Measurements were done at constant applied potentials of 0.4, 0.6, 0.8, and 1.0 V versus RHE in a 0.5 mol L^{-1} H_2SO_4 solution.

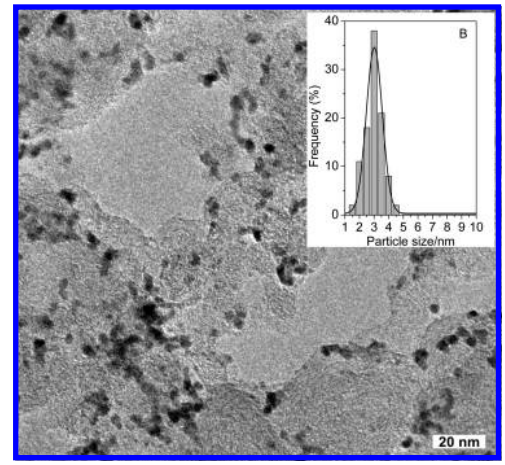

Figure 1. TEM image of Pt−Ru/C catalyst heat treated in nitrogen and particle size distribution histogram.

The general electrochemical behavior was characterized by cyclic voltammetry (CV) in a 0.5 mol L^{-1} H_2SO_4 solution. Electrocatalytic activity for methanol oxidation was evaluated in a 0.5 mol L^{-1} methanol acid solution by linear sweep voltammetry (LSV) and chronoamperometry (CA). All experiments were done at 25 °C in Ar-saturated solutions. Experiments of adsorbed CO oxidation were carried out in the following way. After recording CV in an Ar-purged system, CO was admitted to the cell and adsorbed at 0.15 V versus RHE for 20 min. The excess CO was eliminated with Ar gas, and the adsorbed CO was oxidized at a scan rate of 5 mV s^{-1}.

All electrochemical measurements were performed in a conventional electrochemical cell, with a Pt wire counter electrode placed in a separate compartment and a reversible hydrogen reference electrode. The Pt−Ru/C electrocatalysts were used as ultrathin layers[24] (metal load of 28 μg cm^{-2}) on a glassy carbon disk electrode (0.196 cm^2), previously polished down to 0.3 μm alumina. Pt/C samples prepared in microemulsions and a Pt−Ru/C commercial catalyst were used for comparison.

Solutions were prepared from analytical grade H_2SO_4 (Mallinckrodt), analytical grade methanol (Mallinckrodt), and ultrapure water (Milli-Q, Millipore).

Results and Discussion

Physical Characterization. A typical TEM image and the corresponding histogram of particle size distribution are shown in Figure 1. For all samples, particles were uniformly dispersed on the carbon support, and a narrow particle size distribution was verified. The mean particle size was found to be nearly the

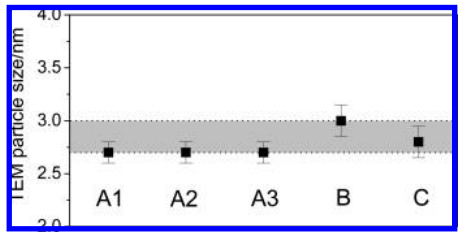

Figure 2. TEM particle size for the Pt−Ru/C catalysts heat treated under different conditions.

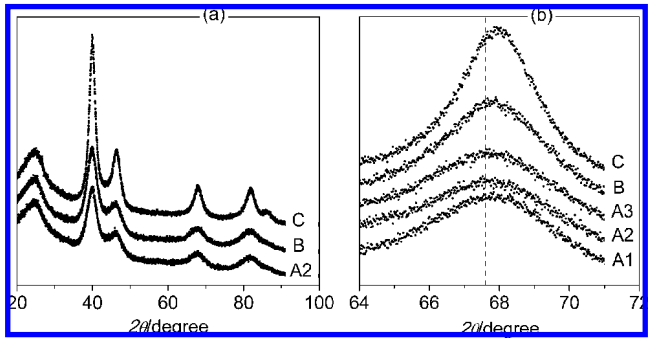

Figure 3. (a) XRD patterns for some Pt−Ru/C catalysts. (b) Diffraction peak (220) of the Pt fcc structure for the Pt−Ru/C catalysts. Dashed line indicates the position of the (220) Pt signal.

same for all Pt−Ru/C nanocatalysts prepared, providing evidence that heat treatment up to 150 °C did not produce significant particle growth as shown in Figure 2.

EDX analysis revealed that the average Pt:Ru atomic ratio was very close to the nominal value (1:1). The diffraction patterns obtained for the Pt−Ru/C catalysts exhibit the typical signals associated with the face-centered cubic (fcc) structure of Pt (JCPDS 4-802) as shown in Figure 3a for some catalysts. In general terms, broad diffraction peaks were observed for all catalysts. Signals that could be assigned to crystalline ruthenium or ruthenium oxides were not observed. Scherrer's equation was used to estimate the mean crystallite size. The (220) peak of the Pt fcc structure at $2\theta \sim 67°$ (Figure 3b) was used for that purpose because the broad signal of the carbon support does not interfere in this region. Similar values of mean crystallite size were found for all of the samples heat treated in air, and larger ones were obtained for catalysts treated in nitrogen and hydrogen.

For all catalysts, the diffraction signals are clearly displaced to larger 2θ values (Figure 3b). The lattice parameter

$$a = \frac{\sqrt{2}\lambda}{\sin\theta} \quad (1)$$

was calculated at a (220) diffraction and, for all Pt−Ru/C catalysts, was smaller than for Pt, indicating a contraction of the lattice due to partial substitution of Pt by Ru in the fcc structure. The amount of alloyed Ru was estimated by Vegard's law, which assumes a linear dependence of the lattice parameter with the Ru concentration[19,25]

$$x_{(\mathrm{Ru})} = \frac{a - a_0}{a_{\mathrm{alloy}} - a_0} \quad (2)$$

where a is the experimental value of the lattice parameter for the Pt−Ru/C catalysts, a_{alloy} is the lattice parameter for a Pt−Ru solid solution of equiatomic composition taken here as 3.866 Å,[26] and a_0 is the lattice parameter of supported Pt equalling

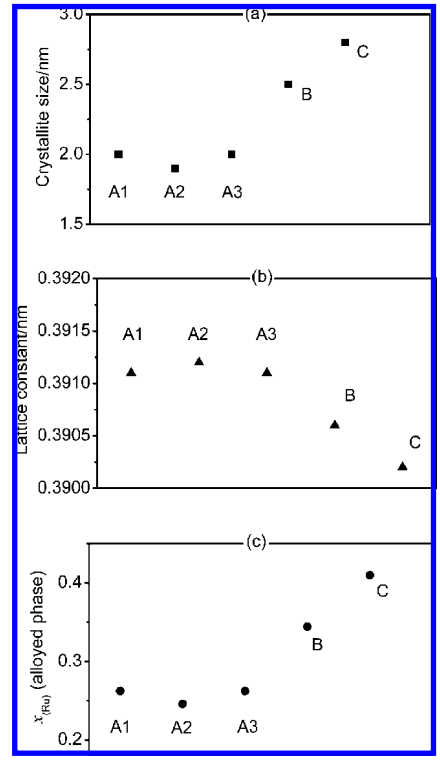

Figure 4. Structural parameters of the Pt−Ru/C nanocatalysts: (a) crystallite size, (b) lattice constant, and (c) amount of Ru in the alloyed phase.

3.927 Å that was determined for Pt/C samples and was found to be in good agreement with literature data.[27]

In general, mean crystallite size as well as lattice parameter and amount of alloyed Ru varied, depending on the heat treatment conditions as shown in Figure 4.

Independent of temperature, the mean crystallite size, lattice parameter, and amount of alloyed Ru show no significant changes for the samples heat treated in air. Treatment at 150 °C in N_2 or H_2 (samples B and C) produced an increase in the average crystallite size, consistent with the increase in the metal phase crystallinity expected to occur around 150 °C in nonoxidant environments.[19] A decrease in the lattice parameter and, consequently, larger amounts of alloyed Ru were observed for samples B and C as expected.

Electrochemical Behavior and Catalytic Activity. The electrochemical properties of the Pt−Ru/C nanocatalysts were first examined by cyclic voltammetry. The curves obtained at 50 mV s^{-1} in an Ar-saturated 0.5 mol L^{-1} H_2SO_4solution, in the potential range of 0.05−0.8 V, are shown in Figure 5. The curve obtained for the Pt/C prepared by the same microemulsion method (inset) serves as evidence that the washing procedure adopted for removal of synthesis residues was efficient and produced clean particles.

The voltammetric profiles have similar shapes for all of the Pt−Ru/C catalysts and involve nearly the same charges, except for catalyst C. The inhibition of the hydrogen peaks, compared with Pt/C, provides evidence for the presence of Ru on the surface, which leads to oxygenated Ru species in low potentials. The broadening of the double-layer region arises from the pseudocapacitive contribution to the double layer charging currents of superficial Ru, either alloyed or segregated as a metal or oxide.[28]

Figure 6 shows the current−potential curves of oxidation of CO adsorbed onto the different Pt−Ru/C catalysts. Sample C

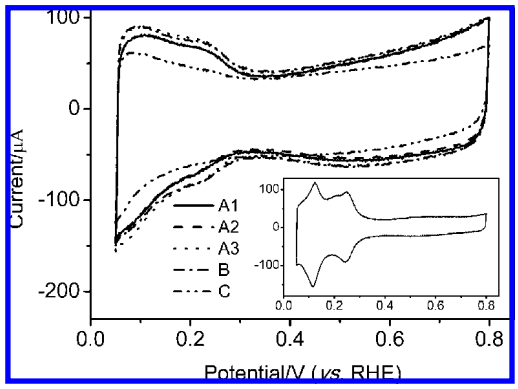

Figure 5. Cyclic voltammetry curves of Pt−Ru/C nanocatalysts obtained at 50 mV s^{-1} in a 0.5 mol L^{-1} H_2SO_4 solution. Inset shows the curve of Pt/C prepared by the same microemulsion method.

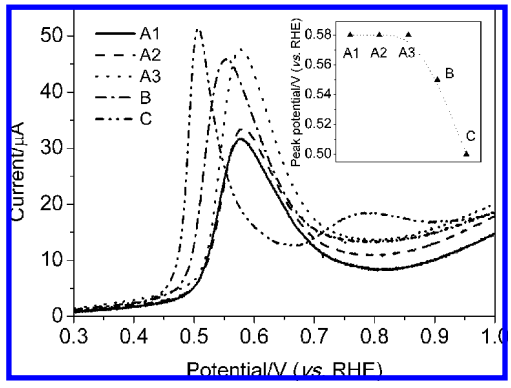

Figure 6. Current−potential curves of the oxidation of adsorbed CO recorded at 5 mV s^{-1} in a 0.5 mol L^{-1} H_2SO_4 solution. Pt−Ru/C catalysts are indicated. Inset shows the peak potential of adsorbed CO oxidation.

has the largest electrocatalytic activity toward CO oxidation, evidenced by the lower onset and peak potentials, while the lowest activities are observed for samples treated in air that have similar behavior. In addition, a significant growth of the electrochemical active areas is apparent for the Pt−Ru/C catalyst treated at 150 °C, probably caused by the increase in the metal phase crystallinity.[19] The trend in activity observed (inset of Figure 6) follows closely the amounts of alloyed Ru determined from the XRD data.

Cyclic voltammetry curves for methanol oxidation (not shown) revealed that the activity of the Pt−Ru/C catalysts is strongly influenced by their surface properties. In general, currents were larger for samples A3 and B and significantly smaller for sample C. Current−time curves for methanol oxidation taken at 0.5 V, normalized by the active area determined from the charge of oxidation of adsorbed CO assuming that the CO coverage for Pt−Ru is identical to that of Pt (420 μC cm^{-2}),[10] are shown in Figure 7. In agreement with CV data, comparison of catalysts treated in air show that catalysts A1 and A2 are less active than catalyst A3. This difference might result from the restructuring of hydrous Ru oxides (loss of water) and the increase of crystallinity of the metallic phase that take place at 150 °C.[19,20] Catalyst B showed the best results for methanol oxidation. A considerable decrease in the electrocatalytic activity was observed for sample C, which is in agreement with previous findings.[19] This drop in performance after heat treatment in hydrogen provided evidence that oxygenated Ru species favor methanol oxidation. It is also worth noting that all of the Pt−Ru/C catalysts prepared in this work,

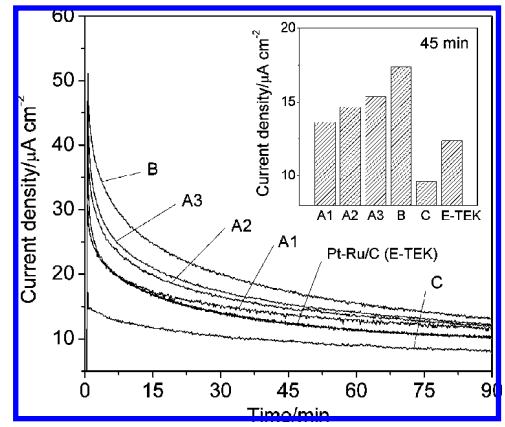

Figure 7. Current−time curves for methanol oxidation obtained at 0.5 V for Pt−Ru/C catalysts. A curve for a Pt−Ru/C commercial catalyst (E-TEK) is included for comparison. Electrolyte is 0.5 mol L^{-1} methanol and 0.5 mol L^{-1} H_2SO_4. Inset shows the current densities at 45 min.

except catalyst C, showed larger current densities compared to that of the Pt−Ru/C commercial catalyst (E-TEK).

The results show that both reactions, the oxidation of adsorbed CO and methanol, are very sensitive to surface properties. However, it must be noted that very different effects are observed in each case.

For the oxidation of adsorbed CO on the different Pt−Ru/C catalysts, the peak potentials are shifted to lower values as the amount of the alloyed phase increases. Catalyst C presented the best catalytic performance, and it is significantly better for the oxidation of adsorbed CO than catalyst B, as revealed by a difference of about 50 mV for peak potentials (Figure 6).

On the other hand, the same tendency is not observed for methanol oxidation. Catalyst C shows the smallest methanol oxidation currents, while on catalyst B, which has less alloy and some oxides, currents are notably larger (Figure 7).

In summary, one the most interesting points of this work is that the results obtained clearly provide evidence that the most efficient catalyst for methanol oxidation is not unavoidably a good catalyst for oxidation of adsorbed CO.

XPS and DXAS Analysis. Because catalysts B and C exhibited the larger and smaller activities for methanol oxidation, respectively, they were chosen to carry out XPS and DXAS studies aiming to correlate their markedly dissimilar catalytic performances with differences in their surface compositions and electronic characteristics. For the sake of simplicity, the as-prepared A1 sample was chosen as the reference sample.

The Pt 4f and Ru 3p high-resolution XPS spectra for samples A1, B, and C are shown in Figure 8. The Pt 4f spectrum was deconvoluted into three doublets, which correspond to Pt $4f_{7/2}$ and Pt $4f_{5/2}$ of different oxidation states. The line with major intensity centered at 71.8 eV can be assigned to Pt in the zero-valence metallic state, shifted toward higher values with respect to the literature value of 71.2 eV.[29] A slight shift of the Pt(0) peak to higher binding energies is a known effect of small particles.[30] Also, peak shifts toward higher values of binding energies for the Pt $4f_{7/2}$ in relation to pure Pt have been reported for carbon-supported[31] and zeolite-supported Pt[32] as well as for Pt nanoparticles dispersed on RuO_2 matrixes,[33,34] and they have been interpreted as being caused by Pt-support interactions. The binding energies of the Pt $4f_{7/2}$ components centered at 72.7−72.9 eV and 74.5−75.9 eV can be attributed to the Pt(II) and Pt(IV) species, respectively.[29]

The binding energies obtained for the components of the Pt $4f_{7/2}$ peak are shown in Table 2 together with the atomic

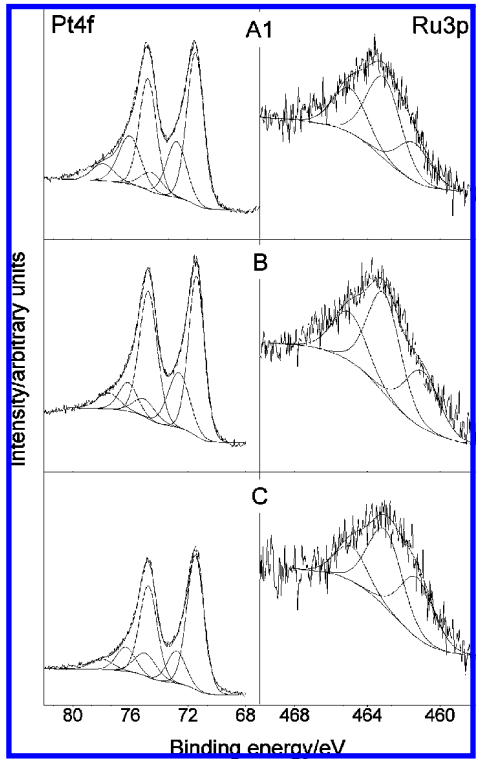

Figure 8. Pt 4f and Ru 3p XPS spectra for Pt−Ru/C catalysts.

TABLE 2: Binding Energies of the Pt $4f_{7/2}$ Components for the Pt−Ru/C Catalysts and Atomic Percentage for Each Signal

catalyst A1	catalyst B	catalyst C	assignment[30]
71.5(60)	71.4(66)	71.5(69)	Pt(0)
72.8(29)	72.6(24)	72.8(18)	Pt(II)−$Pt(OH)_2$
74.5(11)	75.0(10)	75.0(13)	Pt(IV)−PtO_2, $PtO_2 \cdot nH_2O$

TABLE 3: Binding Energies of the Ru $3p_{3/2}$ Components for the Pt−Ru/C Catalysts and Atomic Percentage for Each Signal

catalyst A1	catalyst B	catalyst C	assignment[29,35]
461.4(23)	461.2(28)	461.3(35)	Ru(0)
463.1(50)	463.1(47)	463.0(46)	Ru(IV)−RuO_2
465.0(27)	465.0(24)	464.9(19)	hydrous Ru oxides (RuO_xH_y)

percentage for each signal. In general, Pt is found in the zero-valence state and in ionic form, most likely as $Pt(OH)_2$ and PtO_2. The data also provide evidence that heat treatments at 150 °C in nitrogen and hydrogen (samples B and C) produce an increase in the amount of metallic Pt, while the quantity of hydrated oxides decreases.

As the binding energy for the 3d line of Ru in the zero-valence state (284.3 eV)[29] is very close to the C 1s line, the Ru 3p spectrum was used instead for the analysis of the Ru oxidation states. The Ru $3p_{3/2}$ signal was deconvoluted into three different peaks. Table 3 shows the binding energies and the atomic percentage for each signal.

The first line centered at 461.2−461.4 eV can be attributed to Ru in the zero-valence state. While the second line (463.0−463.1) can be assigned to the Ru(IV) species, the third signal is likely to be due to Ru−O speciation and can be assigned to hydrous Ru oxides RuO_xH_y as suggested in the literature.[20,35] As is seen in Table 3, the amount of Ru in the zero-valence metallic state is larger for samples B and C compared to the as-prepared catalyst A1.

To give a definite interpretation of these peak components is beyond the scope of this work. What really matters to this work is that, in a general manner, the XPS data show that heat treatment at 150 °C produces an increase in the amount of metallic Pt and Ru. This is in excellent agreement with the XRD results that show diffraction peaks shifted to higher 2θ values for those catalysts (Figure 3b), which suggest larger amounts of an alloyed phase. Altogether, data from XRD and XPS show that heat treatment in nitrogen (sample B) produces an increase in the metallic content and degree of alloying, while Ru oxides are partially removed. Treatment in hydrogen (sample C) produces a larger amount of alloy and a more significant removal of Ru oxides as expected.

Dispersive X-ray absorption spectroscopy (DXAS) was used to probe the electronic characteristics of electrocatalysts under in situ electrochemical conditions. The analysis of white lines was performed by using the method of Shukla et al.[36,37] The absorption spectra were fitted by an arc tangent function, which was subtracted from the experimental data, and the result was fitted by a Lorentzian function. The Levenberg−Marquardt nonlinear regression method[38] was used in both fitting procedures.

Figure 9 shows the normalized Pt L_3 absorption edges for the different Pt−Ru/C catalysts. In general, all samples showed an increase in the white line intensity for increasing applied potentials, resulting from the adsorption of oxygenated species onto the Pt surface, which is in agreement with literature reports.[39,40] The largest white line intensity is always observed for sample B (treated in nitrogen), while the white line intensity for catalyst C (treated in hydrogen) is slightly smaller than that for the as-prepared A1 material. Furthermore, at any applied potential, the integrated intensity of the Lorentzian follows the same trend, increasing from A1 to B and exhibiting the smallest value for catalyst C.

To interpret these DXAS results, we must remember that an increase in the amount of alloying would produce a larger white line intensity, which is usually interpreted in terms of the lesser occupancy of the Pt d band caused by the presence of metallic Ru. On the other hand, adsorbed oxygenated species also produce a lesser occupancy of the Pt d band, leading to an increase of the white line intensity. Hence, the intensity increase from sample A1 to sample B is consistent with the increase in the degree of alloying evidenced by the XRD and XPS data. On the other hand, the smallest white line intensity observed for catalyst C would result from the combination of two opposite effects: the increase of alloying and the significant decrease in the amount of oxides. Catalyst B presented the higher integrated intensities of the Lorentzian at any applied potential, which would indicate that the d band of this catalyst is the lesser filled d band compared to those of the other samples.

At present, the most accepted interpretation for the enhanced activity for methanol oxidation on Pt−Ru alloys is based on the bifunctional mechanism,[41] where the methanol molecule is dehydrogenated at the Pt sites, and the Ru sites activate water molecules acting as the oxygen source for the oxidation of CO-like species.[16] In other words, the improved catalytic activity for methanol oxidation would be due to the ability of Ru to supply the oxygenated species (oxide or hydroxide) necessary to oxidize the methanolic residues in low potentials. Additionally, a number of published data indicate that oxidized Ru species play an important role in the electrocatalysis of methanol oxidation.[8,19,20,33,34] It has been proposed that considerable amounts of oxidized phases such as RuO_xH_y are necessary to achieve high activity for methanol oxidation, pointing out that the essence of the bifunctional mechanism does not change by

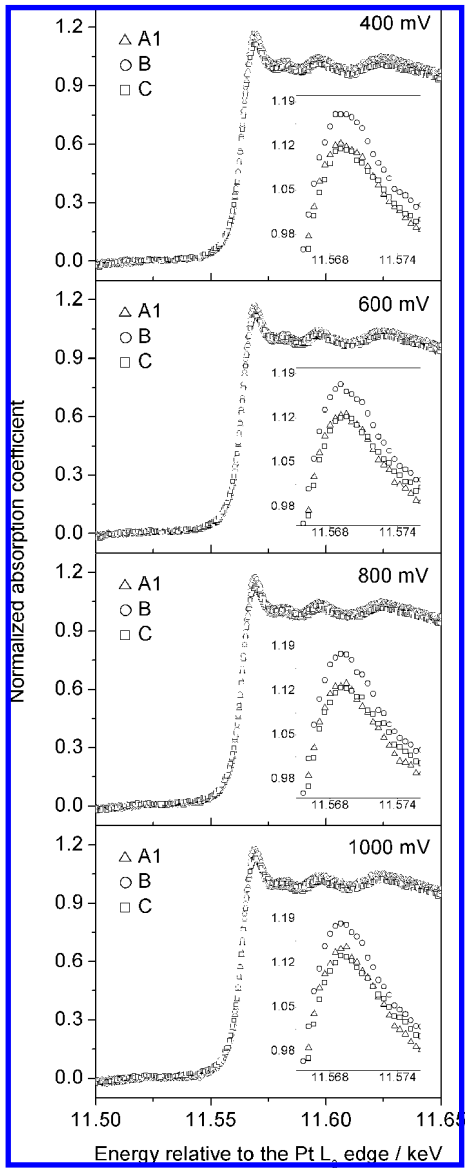

Figure 9. Normalized Pt L_3 absorption edges for different samples and applied potentials as indicated.

substituting Ru for a hydrous ruthenium oxide component.[20,42] Moreover, studies on materials containing Pt nanoparticles dispersed on RuO_2 layers showed an increased electrocatalytic activity for methanol oxidation compared to that of Pt.[33,34]

Yet, adsorption of the intermediates onto the catalyst surface involves transference of charge either to or from the catalyst metal. Hence, the electronic properties of the catalyst should also have a crucial role in this process. DXAS results show that there are significant electronic effects. In general, a partially empty d band should result in the weakening of the bond of CO-like species on the Pt sites. Thus, the enhanced activity presented by sample B, for which the d band is the lesser filled, could be understood as resulting at least partially from the weakening of the bond of CO-like species. Equally, if the amount of the alloyed phase is increased but at the same time there is significant oxide removal, the d band filling would result from the combination of these two opposite effects as seems to be the case for the lowering of the integrated intensity of the Lorentzian and the decrease in catalytic activity for methanol oxidation observed for sample C.

However, if catalytic activity were solely determined by these electronic effects, then the same tendency should be observed for the oxidation of adsorbed CO. Figure 6 clearly shows that this is not the case because CO oxidation follows the same trend as that of the amount of the Pt−Ru alloyed phase. From studies of CO electro-oxidation on Ru-modified Pt(111), Davies et al.[43]proposed that the kinetics of the oxidation of CO taking place through a Langmuir−Hinshelwood mechanism would be fast for Pt sites neighboring Ru clusters and slow for Pt sites that lay at least one atom of Pt away from the Ru sites. Thus, the changes in the onset and peak potentials of CO oxidation shown in Figure 6 could in principle be seen as reflecting an increase in the number of Pt sites neighboring Ru as the degree of alloying increases. Consequently, the most important parameter appears to be the distance between Ru and Pt sites on the catalysts surfaces, i.e., the sites where the oxygenated species are produced, and those where CO is oxidized. Because the removal of oxides does not have an effect on CO oxidation, the catalytic activity for the removal of adsorbed CO seems mostly determined by the number of Pt sites neighboring Ru, while any contributions of the oxide phase to provide oxygenated species and/or through electronic effects are negligible.

It is also important to point out that the increase in the amount of Ru in the alloyed phase is not large enough to have an effect on the methanol dissociative chemisorption by dilution of the Pt sites. It should be kept in mind that the reference for the alloyed phase used to calculate the fraction of alloyed Ru with eq 2 is the equiatomic Pt−Ru solid solution. Indeed, the compositions of the alloyed phase in our catalysts lay between 10−20% Ru, which are within the composition range of 10−40% suggested by Iwasita et al.[5]as the one in which the surface composition of alloys is not a limiting factor for methanol oxidation. In addition, Krausa et al.[44]demonstrated, using differential electrochemical mass spectrometry (DEMS), that the dissociation of methanol to form CO (and/or CO-like species) can take place at relatively low potentials, beginning at 0.15 V and giving a well-defined maximum at 0.25 V for Pt. The same authors found that in the presence of electrodeposited Ru the dissociative adsorption was shifted 50 mV toward more negative potentials. In other words, methanol dissociation and the blocking of the surface with CO and other partially dehydrogenated species take place immediately. Hence, it is unlikely that the dissociative adsorption of methanol is the rate-determining step in the range of potentials of the present study. Furthermore, from studies of methanol oxidation on Pt−Ru materials by electrochemical techniques and in situ FTIR, Iwasita et al.[5]also concluded that the reaction between adsorbed intermediates and adsorbed OH must be responsible for the rate of the process in potentials between 0.35 and 0.6 V.

On those grounds, it seems reasonable to conclude that the presence of oxidized species benefits the methanol oxidation reaction because they produce an electronic effect as evidenced by DXAS results at the same time that RuO_xH_y would provide oxygenated species that facilitate the oxidation of CO-like intermediates. Thus, the enhanced activity for methanol oxidation presented by sample B can be understood as the consequence of the hydrous Ru oxide acting as a donor of oxygenated species and of an electronic effect promoting the weakening of the bond of CO-like species. Nonetheless, the extent of these contributions remains unclear. On the other hand, the significant loss of activity for methanol oxidation observed for the Pt−Ru/C catalyst heat treated in hydrogen (sample C) could also be attributed to the larger removal of hydrous Ru oxides from the catalyst surface.

The importance of oxidized Ru species in the electrocatalysis of methanol oxidation has already been pointed out.[8,19,20,33,34]

Yet, because our previous work[19] showed that the amounts of oxide and alloyed phases are size dependent, it is important to emphasize that the present study was carried out on a Pt−Ru/C catalyst having nearly the same particle size. To the best of our knowledge, no other work has compared the oxidation of methanol on Pt−Ru/C materials with the same particle size and with oxide and alloy phases present in different amounts.

In summary, while it is obvious from the results presented here that the catalytic activity for the oxidation of methanol is somewhat improved by the increase of the alloying degree, it is likewise evident that the presence of oxides seems to be essential for enhancing the electrocatalysis of methanol oxidation. Thus, the oxidation of methanol appears to be related to the d band occupancy as well as to the presence of oxygen donor species. Conversely, the performance of the Pt−Ru/C catalysts for adsorbed CO oxidation appears to follow the amount of the Pt−Ru alloyed phase. Altogether, the data presented here show that the best catalyst for oxidation of adsorbed CO is not necessarily the best one for methanol oxidation.

Without a doubt, oxidation of adsorbed CO and of methanol can be essentially different. For instance, studies of the yields of soluble products of methanol oxidation by using high-performance liquid chromatography (HPLC) have shown that methanol oxidation on Pt produces large amounts of formaldehyde and formic acid.[45,46] and that only 10−20% of the measured charge might be directly related to the CO pathway.[45] Therefore, methanol oxidation currents cannot be ascribed solely to oxidation via adsorbed CO. It must be admitted that oxidation of CO-like species that lead to formaldehyde and formic acid might be substantially different from adsorbed CO oxidation. Hence, while CO stripping can be used to probe the ability for CO oxidation, it cannot be directly related to the ability for removal of CO-like species formed by methanol oxidation. The best catalyst for adsorbed CO oxidation may not be the most efficient for methanol oxidation because these two processes can be very different, depending on the pathways through which methanol oxidation occurs.

Conclusions

Pt−Ru/C nanocatalysts heat treated in different atmospheres under mild conditions show different amounts of Ru oxides and different degrees of alloying and, consequently, different catalytic activity toward methanol oxidation. This study, carried out in the absence of particle size effects, provides evidence that the presence of oxides is essential for the electrocatalysis of methanol oxidation. The largest enhancement appears to be associated with the presence of a hydrous Ru oxide acting as a donor for an oxygenated species, combined with an electronic effect promoting the weakening of the bond of a CO-like species.

The properties of Pt−Ru/C catalysts such as the amount of oxides, degree of alloying, and d band occupancy have different effects on the electrocatalytic activity for methanol oxidation than for adsorbed CO oxidation. Therefore, the most efficient catalyst for methanol oxidation is not necessarily the best for oxidation of adsorbed CO.

Acknowledgment. The authors thank the Brazilian Agencies Fundação de Amparo à Pesquisa do Estado de São Paulo (FAPESP, 07/54434-0), the Conselho Nacional de Desenvolvimento Científico e Tecnológico (CNPq, 480662/2007-0), and the Financiadora de Estudos e Projetos (FINEP, 01.06.0939.00) for financial support and the Brazilian Synchrotron Light National Laboratory (LNLS) for assisting with the DXAS measurements. The authors also thank Prof. Peter Hammer (IQ-UNESP) for valuable help with the XPS analysis. D.R.M.G. thanks FAPESP (Proc. 06/60769-2), and J.P. thanks CNPq (Proc. 382986/2007-5) for the fellowships granted.

References and Notes

(1) Vielstich, W.; Lamm, A.; Gasteiger, H. A. *Handbook of Fuel Cells: Fundamentals, Technology, and Applications*; Wiley: Chichester, U.K. and Hoboken, NJ, 2003.
(2) Srinivasan, S. *Fuel Cells: From Fundamentals to Applications*; Springer: New York, 2006.
(3) Lamy, C.; Lima, A.; LeRhun, V.; Delime, F.; Coutanceau, C.; Leger, J. M. *J. Power Sources* **2002**, *105*, 283.
(4) Kelley, S. C.; Deluga, G. A.; Smyrl, W. H. *Electrochem. Solid State Lett.* **2000**, *3*, 407.
(5) Iwasita, T.; Hoster, H.; John-Anacker, A.; Lin, W. F.; Vielstich, W. *Langmuir* **2000**, *16*, 522.
(6) Hoster, H.; Iwasita, T.; Baumgartner, H.; Vielstich, W. *Phys. Chem. Chem. Phys.* **2001**, *3*, 337.
(7) Lizcano-Valbuena, W. H.; Paganin, V. A.; Gonzalez, E. R. *Electrochim. Acta* **2002**, *47*, 3715.
(8) Lasch, K.; Jorissen, L.; Friedrich, K. A.; Garche, J. *J. Solid State Electrochem.* **2003**, *7*, 619.
(9) Seller, T.; Savinova, E. R.; Friedrich, K. A.; Stimming, U. *Electrochim. Acta* **2004**, *49*, 3927.
(10) Bock, C.; MacDougall, B.; LePage, Y. *J. Electrochem. Soc.* **2004**, *151*, A1269.
(11) Wang, K.; Gasteiger, H. A.; Markovic, N. M.; Ross, P. N. *Electrochim. Acta* **1996**, *41*, 2587.
(12) Gotz, M.; Wendt, H. *Electrochim. Acta* **1998**, *43*, 3637.
(13) Choi, J. H.; Park, K. W.; Kwon, B. K.; Sung, Y. E. *J. Electrochem. Soc.* **2003**, *150*, A973.
(14) Neto, A. O.; Perez, J.; Napporn, W. T.; Ticianelli, E. A.; Gonzalez, E. R. *J. Braz. Chem. Soc.* **2000**, *11*, 39.
(15) Mukerjee, S.; Urian, R. C.; Lee, S. J.; Ticianelli, E. A.; McBreen, J. *J. Electrochem. Soc.* **2004**, *151*, A1094.
(16) Iwasita, T. *Electrochim. Acta* **2002**, *47*, 3663.
(17) Ishikawa, Y.; Liao, M. S.; Cabrera, C. R. *Surf. Sci.* **2000**, *463*, 66.
(18) Antolini, E. *Mater. Chem. Phys.* **2003**, *78*, 563.
(19) Godoi, D. R. M.; Perez, J.; Villullas, H. M. *J. Electrochem. Soc.* **2007**, *154*, B474.
(20) Rolison, D. R.; Hagans, P. L.; Swider, K. E.; Long, J. W. *Langmuir* **1999**, *15*, 774.
(21) Wendlandt, W. W. *Thermal Analysis,* 3rd ed.; Wiley: New York, 1986.
(22) Tolentino, H. C. N.; Cezar, J. C.; Watanabe, N.; Piamonteze, C.; Souza-Neto, N. M.; Tamura, E.; Ramos, A.; Neueschwander, R. *Phys. Scr.* **2005**, *T115*, 977.
(23) Mc Breen, J.; O'Grady, W. E.; Pandya, K. I.; Hoffman, R. W.; Sayers, D. E. *Langmuir* **1987**, *3*, 428.
(24) Schmidt, T. J.; Gasteiger, H. A.; Stab, G. D.; Urban, P. M.; Kolb, D. M.; Behm, R. J. *J. Electrochem. Soc.* **1998**, *145*, 2354.
(25) Cullity, B. D. *Elements of X-ray Diffraction*, 2nd ed.; Addison-Wesley Publishing Co.: Reading, MA, 1978.
(26) Villars, P.; Calvert, L. D. *Pearson's Handbook of Crystallographic Data for Intermetallic Phases*, 2nd ed.; ASM International: Materials Park, OH, 1991.
(27) Beard, B. C.; Ross, P. N. *J. Electrochem. Soc.* **1990**, *137*, 3368.
(28) Trasatti, S.; Buzzanca, G. *J. Electroanal. Chem.* **1971**, *29*, A1.
(29) Moulder, J. F.; Chastain, J. *Handbook of X-ray Photoelectron Spectroscopy: A Reference Book of Standard Spectra for Identification and Interpretation of XPS Data*; Physical Electronics Division, Perkin-Elmer Corp.: Eden Prairie, MN, 1992.
(30) Roth, C.; Goetz, M.; Fuess, H. *J. Appl. Electrochem.* **2001**, *31*, 793.
(31) Antolini, E.; Giorgi, L.; Cardellini, F.; Passalacqua, E. *J. Solid State Electrochem.* **2001**, *5*, 131.
(32) Vedrine, J. C.; Dufaux, M.; Naccache, C.; Imelik, B. *J. Chem. Soc., Faraday Trans. 1* **1978**, *74*, 440.
(33) Villullas, H. M.; Mattos-Costa, F. I.; Bulhões, L. O. S. *J. Phys. Chem. B* **2004**, *108*, 12898.
(34) Villullas, H. M.; Mattos-Costa, F. I.; Nascente, P. A. P.; Bulhões, L. O. S. *Chem. Mater.* **2006**, *18*, 5563.
(35) Yang, C. W.; Wang, D. L.; Hu, X. G.; Dai, C. S.; Zhang, L. *J. Alloys Compd.* **2008**, *448*, 109.
(36) Shukla, A. K.; Raman, R. K.; Choudhury, N. A.; Priolkar, K. R.; Sarode, P. R.; Emura, S.; Kumashiro, R. *J. Electroanal. Chem.* **2004**, *563*, 181.
(37) Sousa, R.; Colmati, F.; Ciapina, E. G.; Gonzalez, E. R. *J. Solid State Electrochem.* **2007**, *11*, 1549.

(38) Marquardt, D. W. *J. Soc. Ind. Appl. Math.* **1963**, *11*, 431.
(39) Herron, M. E.; Doyle, S. E.; Pizzini, S.; Roberts, K. J.; Robinson, J.; Hards, G.; Walsh, F. C. *J. Electroanal. Chem.* **1992**, *324*, 243.
(40) Hwang, B. J.; Tsai, Y. W.; Lee, J. F.; Borthen, P.; Strehblow, H. H. *J. Synchrotron Radiat.* **2001**, *8*, 484.
(41) Watanabe, M.; Motoo, S. *J. Electroanal. Chem.* **1975**, *60*, 267.
(42) Long, J. W.; Stroud, R. M.; Swider-Lyons, K. E.; Rolison, D. R. *J. Phys. Chem. B* **2000**, *104*, 9772.
(43) Davies, J. C.; Hayden, B. E.; Pegg, D. J.; Rendall, M. E. *Surf. Sci.* **2002**, *496*, 110.
(44) Krausa, M.; Vielstich, W. *J. Electroanal. Chem.* **1994**, *379*, 307.
(45) Batista, E. A.; Malpass, G. R. P.; Motheo, A. J.; Iwasita, T. *Electrochem. Commun.* **2003**, *5*, 843.
(46) Batista, E. A.; Malpass, G. R. P.; Motheo, A. J.; Iwasita, T. *J. Electroanal. Chem.* **2004**, *571*, 273.

JP8108804